Phase Transition and Criticality of Methane Confined in Nanopores

Huan Yang,[a] Kevin Jayaatmaja,[b] Morteza Dejam,[a] Sugata P. Tan,[c] Hertanto Adidharma[a,b]

[a]Department of Petroleum Engineering, College of Engineering and Applied Science, University of Wyoming, 1000 E. University Avenue, Laramie, WY 82071-2000, USA

[b]Department of Chemical Engineering, College of Engineering and Applied Science, University of Wyoming, 1000 E. University Avenue, Laramie, WY 82071-2000, USA

[c]Planetary Science Institute, Tucson, Arizona 85719-2395, USA

Abstract

For the first time, the phase transition and criticality of methane confined in nanoporous media are measured. The measurement is performed by establishing an experimental setup utilizing a differential scanning calorimeter (DSC) capable of operating under very low temperatures as well as high pressures to detect the capillary phase transition of methane inside nanopores. By performing experiments along isochoric cooling paths, both the capillary condensation and the bulk condensation of methane are detected. The pore critical point (PCP) of nanoconfined methane is also determined and then used to derive the parameters of a previously developed self-consistent equation of state based on the Generalized van der Waals (vdW) partition function. Using this parameter, the equation of state can predict the capillary-condensation curves that agree well with the experimental data.

1. Introduction

Nanoporous media are becoming more important nowadays with potential applications widely ranging from energy and environment to biology and medicine. Examples are the extensive applications of nanoporous media in drug delivery,[1] catalysis,[2] separation,[3] surface and subsurface gas storage,[4,5] and recovery of hydrocarbons from unconventional reservoirs.[6] The current limited understanding of the behavior of fluids under nanoconfinement has largely restricted the research and development in these areas.

In particular, the phase transition of nanoconfined fluids is of great scientific interest because its enhanced understanding can improve our knowledge regarding the adsorption processes, the fluid-fluid interactions, and the fluid-pore wall interactions under nanoconfinement.[7-9] The pore critical point (PCP) data are also needed for modeling purposes; PCP is a point beyond which no phase transition can occur in pores. Several equations of state (EOS), which have been developed in recent years to describe the phase behavior for nanoconfined fluids, are dependent on the PCP data to derive their parameters.[10-12]

Numerous experimental works have been performed on the phase transition of various fluids under nanoconfinement. The experimental methods that exist in the literature for measuring the phase transition of nanoconfined fluids include calorimetric,[13 - 20] microfluidic-based,[21]

adsorption-desorption,[22] and X-ray scattering methods.[23] However, none of the aforementioned techniques have measured the phase transition of nanoconfined methane, partly due to the extremely low temperature range required, despite the fact that the phase transition of methane confined in nanopores is crucial for the flow simulation of hydrocarbons in unconventional reservoirs (including coal seam gas, shale gas, tight gas, and gas hydrates) as methane is the main component of natural gas. The most relevant experimental work to the phase transition of confined methane in nanoporous media is the measurement of capillary condensation for deuterated methane (CD_4) confined in MCM-41 and SBA-15 at atmospheric pressure using small-angle neutron scattering method by Chiang et al.[24] By measuring deuterated methane adsorption in MCM-41 and SBA-15, they observed that the capillary condensation temperature of deuterated methane isobarically shifted to higher temperature when the pore size was smaller. However, their measurements for capillary condensation of deuterated methane are limited to one bar and deuterated methane may have different phase behavior from methane.

In this work, for the first time, an experimental set up is established using a differential scanning calorimeter (DSC) to measure the phase-transition data of confined methane in MCM-41 and SBA-15 by implementing an isochoric cooling procedure. The cooling procedure has been successfully applied with a micro-DSC in our previous work on other chemicals.[13-18] Since methane is a simple molecule, the measured data can also serve as a benchmark useful for the development and validation of models and simulation results, which is so far missing in the literature. For this reason, the PCP of confined methane is to be determined as well.

There are few methods for determining the PCP of confined fluids from capillary-condensation experiments. Morishige and Nakamura introduced a method for determining the PCP based on the capillary condensation derived from adsorption-desorption isotherms.[25] The PCP was determined from the discontinuity in a plot of the reciprocal of the isotherm slope at capillary condensation against temperature. However, the method is inherently inaccurate due to the subtlety of slope change, while the three-line approach using DSC data, which was introduced by us, has been shown to be accurate.[17]

On modeling side, approaches in the literature include various modified equations of state, which rely on an auxiliary equation, such as the Young-Laplace equation, to include the nanoconfinement effects.[26-28] In some modeling works in petroleum engineering[11,12] to describe confined fluids, PCP has been used to replace the bulk critical point in deriving the parameters of cubic EOS. This latter approach has been shown to be incorrect and unable to account for the effects of confinement.[10] Recently, we developed a self-consistent EOS based on the generalized van der Waals (vdW) partition function, the parameters of which were directly derived from the experimental PCP data. This EOS has been applied to correctly predict the capillary-condensation curves in MCM-41 that match the experimental data.[10] We will also apply the EOS in this paper for its further validation with confined methane.

2. Materials and Apparatus

2.1. Materials

MCM-41 mesoporous silica is purchased from Advanced Chemicals Supplier and SBA-15 mesoporous silica is purchased from Sigma Aldrich. Two standard materials are used to calibrate the BT215 Calorimeter: deionized water and naphthalene. Naphthalene is purchased from Sigma Aldrich, which is of analytical standard grade with a purity higher than 99.7%. Two other standard substances are also used for validation: indium and cyclohexane. Indium is purchased from Goodfellow Corporation with a purity of 99.999%, while cyclohexane is from Fisher Scientific, which is of HPLC grade with a purity higher than 99.99%. Methane gas is of research grade 5.0 with a purity higher than 99.999% purchased from Airgas.

2.2. Apparatus

The equipment for measuring the capillary condensation using isochoric method is shown in Figure 1, the key part of which is the BT 2.15 DSC, purchased from SETARAM Inc., which can operate in a temperature range of −196 to 200℃, scanning rate from 0.01 to 1℃/min, with a pressure limit of 600 bar. The resolution of power detection is 20 μW. The BT 2.15 DSC has a cooling jacket with liquid nitrogen (N_2) as the coolant delivered from TP100 tank. To control and minimize the consumption of liquid N_2, its delivery system is equipped with an automatic switching system. When liquid N_2 in the jacket of BT 2.15 is below a certain level, measured by a liquid level gauge, the automatic switching system will automatically open a solenoid valve and refill the liquid N_2. Reversely, the solenoid valve will be closed if the liquid N_2 level reaches a specific upper limit. The evolution controller is used to acquire and digitize the various calorimetric signals from BT 2.15, and then transfer them to a computer. The instrument is equipped with a sweeping helium gas circuit to prevent the potential condensation of water from moist air inside BT 2.15 during a cooling process.

A tank of model TP100 with a storage capacity of 100 liters from SETARAM Inc. is used to store and deliver liquid N_2 into the jacket of BT 2.15. Two high pressure vessels made of Inconel 625 with pressure and temperature limits up to 600 bar and 500°C have an identical volume of 3.6 cm^3. One of them is the test vessel used to place a test sample while the other is the reference vessel, which is filled with helium gas of 2 bar to prevent any possible condensation of water vapor inside the reference vessel. The pressure of the helium gas inside the reference cell can be any pressure (e.g., 1 bar or 2 bar).

A high-sensitivity digital pressure transducer of model CPT6100 manufactured by MENSOR is used to measure the pressure in the test vessel. The transducer has a measuring range of 0 to 400 bar with an accuracy of 0.01% over full span. The pressure data are acquired synchronously with the heat flow data from BT 2.15. To ensure accurate recordings of the pressure, the distance between the pressure transducer and the test vessel is minimized.

A syringe pump of model 500D from TELEDYNE ISCO, with a cylinder capacity of 507 mL, a flow rate range of 0.001 to 204 mL/min, and a pressure range of 0.7 to 258.6 bar, is used to adjust the initial experimental pressure to a desired value. A vacuum pump of model 1400 from

WELCH is used to remove any remaining gas (e.g., air) inside the adsorbent, test vessel, tubes and syringe pump before injecting methane.

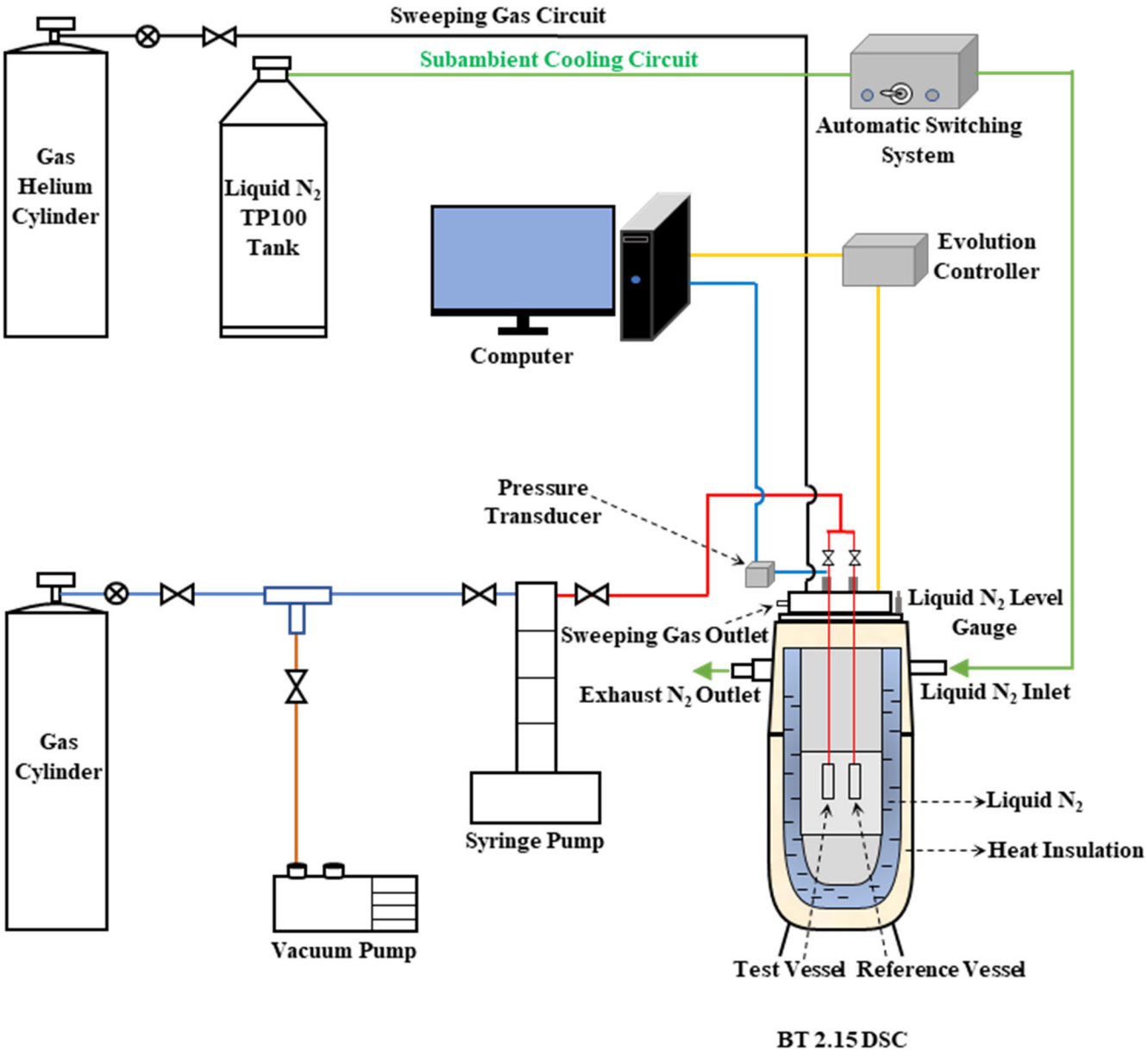

Figure 1. Schematic diagram of experimental setup.

3. Experiments

3.1. Calibration of BT 2.15 DSC

To ensure accurate measurements, the BT 2.15 DSC has been calibrated by measuring the melting points of two standard substances, i.e., naphthalene and deionized water. Firstly, a specific amount of sample (e.g., naphthalene) is weighed, put into the sample cell, and introduced into the DSC. Then, a heating process is conducted with a constant scanning rate, during which an

endothermic heat flow peak of melting is detected. The melting point is the temperature corresponding to the intersect between the heat flow baseline and the tangent of the sharp falling part of the detected heat flow peak, which is commonly known as the onset point. With the same aforementioned procedure, a series of melting points under varying scanning rate ranging from 0.03 to 0.3°C/min is obtained. A total of 8 points are obtained for calibration in this work, i.e., five from naphthalene and three from deionized water. Finally, these values are input into the associated processing software to perform a polynomial regression to obtain the calibration coefficients. For the record, the deionized water is frozen first in a cooling process followed by a heating process to measure the melting point of water. After calibration with deionized water and naphthalene, the measured melting points for frozen deionized water, naphthalene, indium, and frozen cyclohexane are −0.02°C (the literature value is 0°C), 80.13°C (the literature value is 80.05°C), 156.88°C (the literature value is 157°C), and 6.65°C (the literature value is 6.45°C), respectively. All of the literature values are taken from NIST.[29]

To obtain the uncertainty of the DSC measurements in this work, it is important to also check the performance of the instrument in the low temperature range. This is performed by measuring the bulk condensation (vapor pressure) of methane, the accurate data of which are available.[29] As described later, in a single experimental run to measure the condition of capillary condensation, the condition of bulk condensation is also obtained, and therefore no separate measurements for bulk condensation are needed. The determination of the uncertainties of the DSC measurements is given in the Supporting Information.

3.2. Characterization of Mesoporous Silicas

The mesoporous silicas used in this work, i.e., MCM-41 and SBA-15, are characterized using BET (Brunauer-Emmett-Teller) analysis, in which the pore size distribution is determined using NLDFT (Non-Local Density Functional Theory) and the BJH (Barrett–Joyner–Halenda) methods. The equipment and procedure used can be found in our previous work.[18]

3.3. Capillary Condensation Measurements of Methane

The isochoric cooling process to measure the capillary condensation of methane under low temperature condition with BT 2.15 DSC is similar to that adopted in our previous works with micro-DSC.[18,30] The difference is that for BT 2.15 DSC, the syringe pump, which is used primarily for adjusting the initial pressure to a desired value, also plays the role of a volume buffer with a capacity of 507 mL to stabilize the pressure and facilitate the measurement. Small pressure fluctuations in the 3.6-mL test vessel during the cooling process are effectively damped by a much bigger volume of the buffer.

A series of capillary-condensation points is measured starting from a temperature close to the bulk critical temperature to lower temperatures through multiple isochoric cooling processes. A cooling process starts from a specified temperature and pressure in the vapor region and proceeds at a constant cooling rate of 0.05°C/min. Through the whole cooling process, the temperature and heat flow are recorded by the DSC, while the pressure is recorded synchronously

by the pressure transducer. The same procedure is repeated for other start points at lower pressures and temperatures to produce the entire capillary-condensation curve.

3.4. Determination of PCP of Methane

The PCP can be determined using the three-line approach developed in our previous work.[17] In this approach, we plot the inverse of temperature and natural log of pressure at capillary condensation against the released heat. The released heat of capillary condensation is determined from the area of the small capillary-condensation peak on the thermogram, which is automatically obtained by the DSC after identifying the initial and ending points of the peak on the baseline. For a certain amount of nanoporous medium, this plot is linear so that three lines used in the approach represent the measurements using three different amounts of nanoporous medium. The intercept at the vertical axis, i.e., the point at which no heat is released, should be the PCP, which is determined such that the linear regressions of the three lines result in the largest correlation coefficient R^2.

4. Modeling

The modeling is based on the equilibrium between phases in the confinement. The chemical potential is calculated based on the Generalized van der Waals partition function,[10] the parameters of which are directly derived from experimentally measured PCP. The equilibrated phases inside the pore are determined using the Maxwell rule of equal area and the bulk pressure at which capillary condensation occurs is then predicted using the fact that the chemical potential of the confined fluid is equal to that in the bulk, which is calculated from SAFT2 EOS.[10,31] The calculation procedure can be found in Figure S1 in the Supporting Information.

For methane in MCM-41, the original EOS is applied without modification. However, as shown later, the capillary condensation of methane in SBA-15 is not represented well using a temperature-independent parameter C. Therefore, the parameter C, which is related to the reduced volume for the potential well around a fluid molecule in the attractive region, is now proposed to be a function of temperature:

$$C = C_o\left(1 - b\left(\frac{1}{T^*} - \frac{1}{T_{Cp}^*}\right)\right) \tag{1}$$

where b is a correction factor, T_{Cp}^* is the reduced pore critical temperature (= kT_{Cp}/ε), T^* is the reduced temperature (= kT/ε), k is the Boltzmann constant, ε is the well depth of the square-well potential for the fluid-fluid interaction, and C_o is the temperature-independent parameter given by:[10]

$$C_o = \frac{27}{4\rho_{max}^*\left(e^{1/T_{Cp}^*} - 1\right)} \tag{2}$$

where ρ_{max}^* is the maximum reduced density (= $\sqrt{2}$). The value of C needs to become equal to C_o as the temperature goes to T_{Cp}, which is satisfied by the proposed Eq (1). For MCM-41, the

correction factor b is not needed ($b = 0$) to reproduce the original EOS, i.e., when $C = C_0$ at any temperatures.

5. Results and Discussion

5.1. Characterization of MCM-41 and SBA-15

Figure 2(a) shows the measured nitrogen adsorption and desorption isotherms at 77 K. The isotherms of N_2 gas in SBA-15 exhibit type IV(a) with an H1-type hysteresis loop typical of mesoporous adsorbents with mesopores larger than ~4 nm, while MCM-41 is close to reversible type IV(b) without distinct hysteresis loop, which is typical of mesopores of smaller mesopore diameters, according to IUPAC Technical Report.[32] There is no micropores in MCM-41, while we can confirm the existence of micropores in SBA-15 as seen in the pore size distribution in Figure 2(b). The BET specific surface area is determined from the points of relative pressure between 0.1-0.2 on the isotherms, while the total pore volume is determined from the amount of nitrogen adsorbed at a relative pressure of 0.99. The modal diameter of the pores obtained from NLDFT is adopted in this work as it is considered more reliable,[32] which corresponds to the peak of the pore size distribution in Figure 2(b). The pore size evaluated by the BJH method is also included for comparison purposes, which generally underestimates the actual pore size about 20-30% for pore diameter < 10 nm.[32] The properties of the adsorbents are summarized in Table 1.

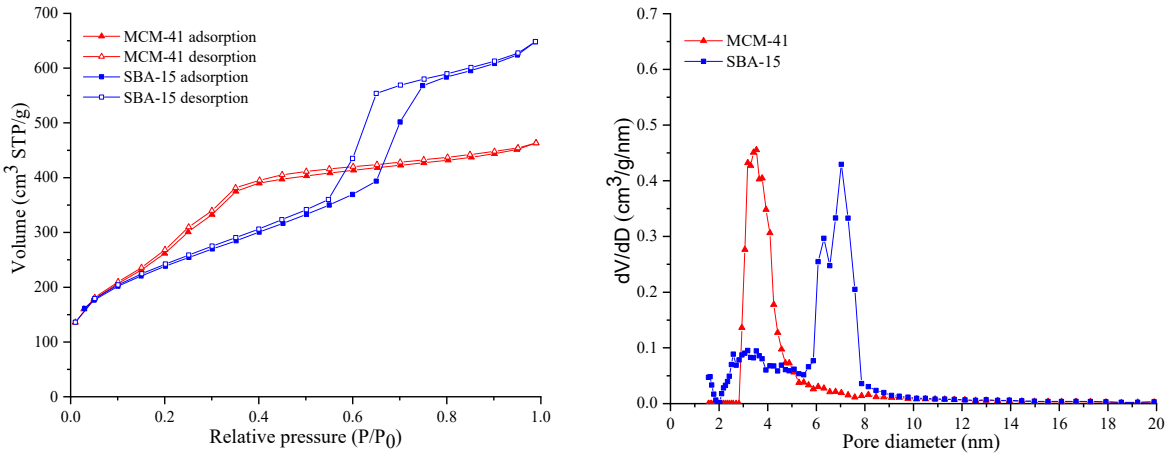

(a) (b)

Figure 2. Characterization of MCM-41 and SBA-15: (a) Nitrogen adsorption and desorption isotherms at 77 K; (b) NLDFT pore size distributions.

Table 1. Properties of the adsorbents from nitrogen adsorption isotherms at 77 K.[§]

Sample	S_{BET}, m^2/g	V_{total}, cm^3/g	D_{BJH}, nm	D_{NLDFT}, nm
MCM-41	980.7	0.762	3.1	3.5
SBA-15	861.9	1.003	5.6	7.0

[§]S_{BET}, multipoint BET surface area; V_{total}, total pore volume; D_{BJH}, modal diameter of pores obtained from the BJH method desorption branch; D_{NLDFT}, modal diameter of pores obtained from the NLDFT method.

5.2. Isochoric Measurement of Capillary Condensation of Methane Confined in MCM-41 and SBA-15

The isochoric method is successfully applied to the measurement of phase transition condition of fluids confined in nanopores at extremely low temperature range. This is demonstrated by the measurement of capillary condensation of methane in MCM-41 and SBA-15. Figure 3 shows typical thermograms where a small distinct exothermic peak of heat flow during the capillary condensation and a large exothermic peak for the bulk condensation are observable. Along a cooling path, the phase transition of confined methane in nanopores is encountered first before that of the bulk methane. The capability of measuring the bulk condensation, the condition of which is widely available in the literature, enables us to determine the measurement uncertainties of capillary condensation.

The pressure and temperature of the capillary condensation are identified from the heat peak on the thermogram by the following procedure. First, the baseline, i.e., the horizontal black line overlapping with the heat flow in Figure 3, is identified. Then, a parallel line to the baseline is drawn tangent to the heat peak. Finally, the capillary-condensation pressure and temperature corresponding to the tangent point can be determined. Therefore, a stable baseline is required during the experiments, which can be made by introducing a volume buffer provided by the syringe pump to stabilize the pressure and thus facilitate the pinpointing of the capillary condensation at distinct small peaks.

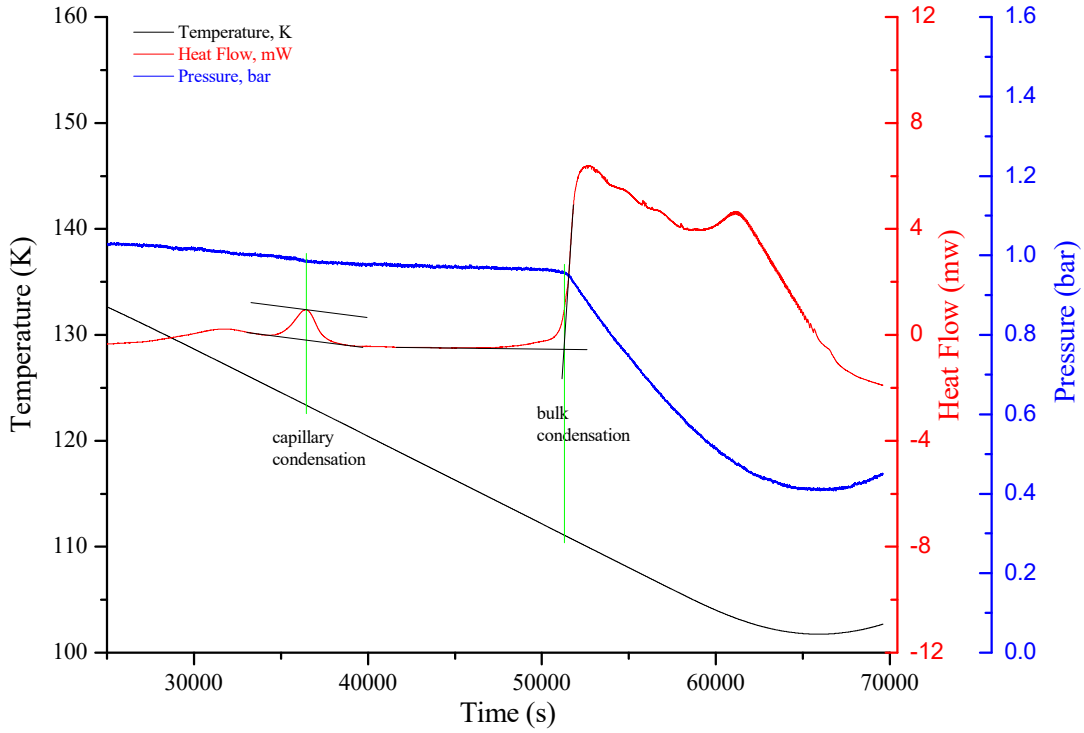

(a)

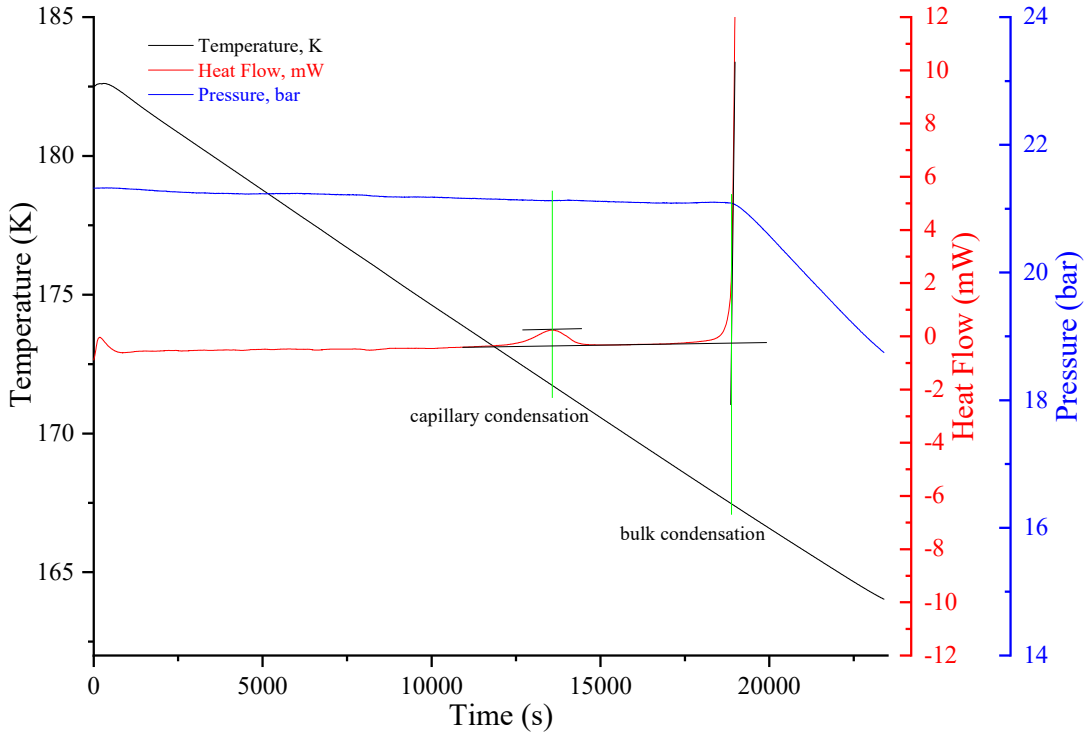

(b)

Figure 3. Typical thermograms of measurement of capillary condensation of methane confined in (a) MCM-41 of 3.5 nm and (b) SBA-15 of 7.0 nm.

The pressure starts to drop sharply when the bulk condensation happens, which occurs when the heat flow starts rising dramatically. As shown in Figure 3, the intersection point of the baseline and the tangent of the sharp rise of heat-flow curve corresponds to the bulk-condensation point. By comparing the measured bulk condensation pressure and temperature with the literature data from NIST,[29] we can determine that the measurement of BT 2.15 DSC is accurate, as shown in Figure 4.

As expected, the P-T diagram in Figure 4 shows that the capillary-condensation curves for both MCM-41 and SBA-15 are below the bulk vapor-pressure curve. In other words, the capillary-condensation pressure of methane in MCM-41 and SBA-15 is isothermally lower compared to the bulk vapor pressure, or equivalently the capillary-condensation temperature is isobarically higher, as also observed for other gases confined in nanopores. In addition, the capillary-condensation curve of methane in MCM-41 shifts farther compared to that in SBA-15 due to the smaller nanopore size of MCM-41. A typical cooling path for a continuous measurement, i.e., when the cooling process is continued even after the bulk condensation has occurred, shows that the measurement for bulk condensation follows the bulk vapor-pressure curve from NIST[30] consistently, and thereby indicates accurate measurements of capillary condensation. The measured capillary-condensation data are given in the Supporting Information.

Like the measurement using the isochoric method with micro-DSC,[18] the cooling path of the measurement is not an ideal isochoric path but a path that slightly lies above it. However, this does not affect the accurate measurement of capillary and bulk condensation. For comparison, literature data of the capillary condensation of deuterated methane (CD_4) in MCM-41 and SBA-15 of similar sizes to ours are included in Figure 4,[24] which shows that the capillary condensation of deuterated methane measured by Chiang et al. is consistent with our work.

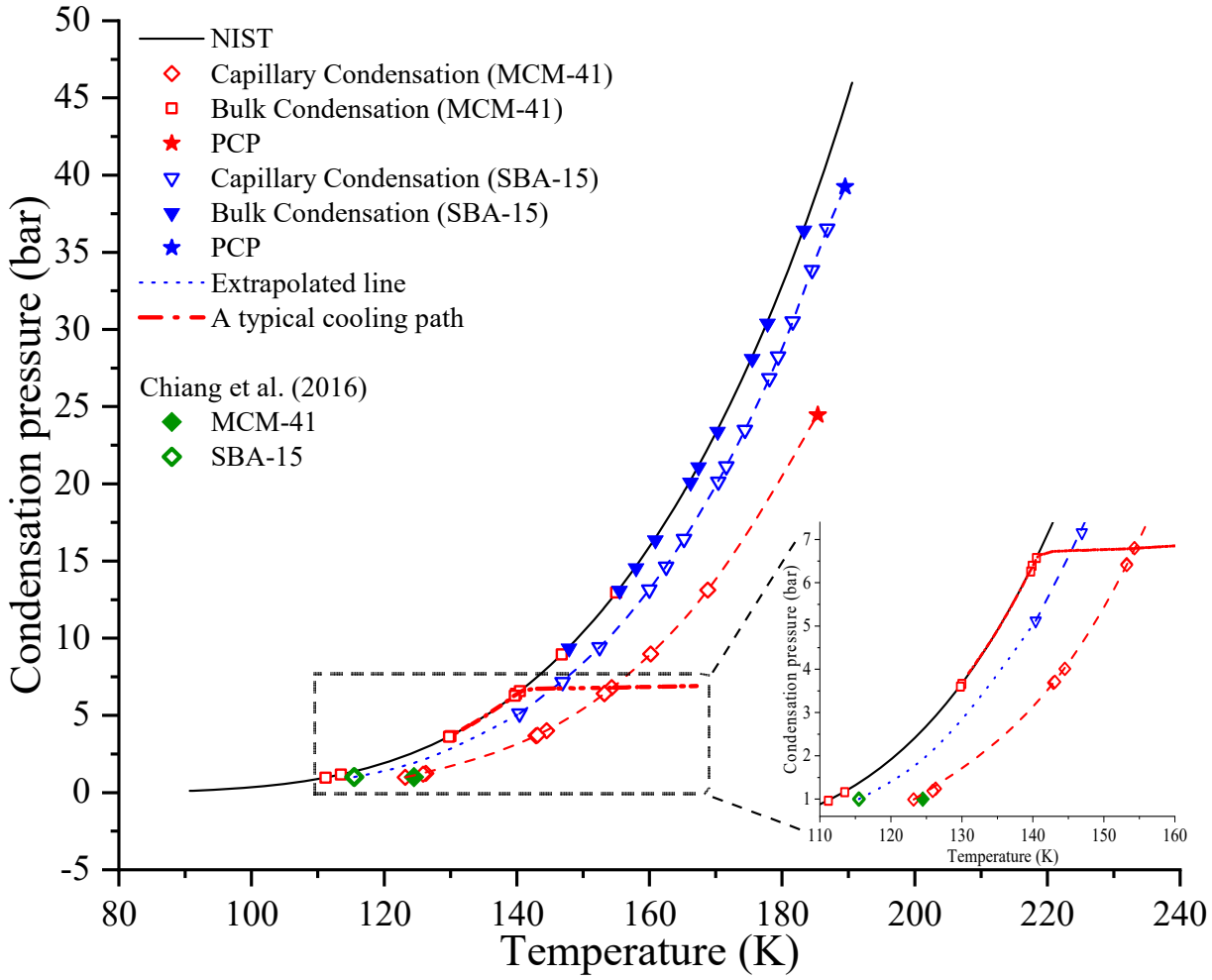

Figure 4. P-T diagram of the capillary condensation of methane confined in MCM-41 (3.5 nm) and SBA-15 (7.0 nm). PCP: pore critical point. Data from Chiang et al.: in MCM-41 (3.30 nm) and SBA-15 (6.82 nm).[24] Dashed curves are just a guide to the eye.

5.3. Criticality of Methane in MCM-41 and SBA-15

Figures 5 and 6 show that the reciprocal of absolute temperature and the logarithm of capillary-condensation pressure versus the total heat of capillary condensation of nanoconfined methane exhibit excellent linearity. The slopes of the lines are dependent on the amount of nanoporous media and all lines will converge to a single point at zero heat of capillary condensation, which is considered as the reciprocal of pore critical temperature and logarithm of pore critical pressure, respectively. With this three-line approach,[17] the PCPs of methane confined in MCM-41 and SBA-15 are determined, the results of which are shown in Table 2 and Figure 4.

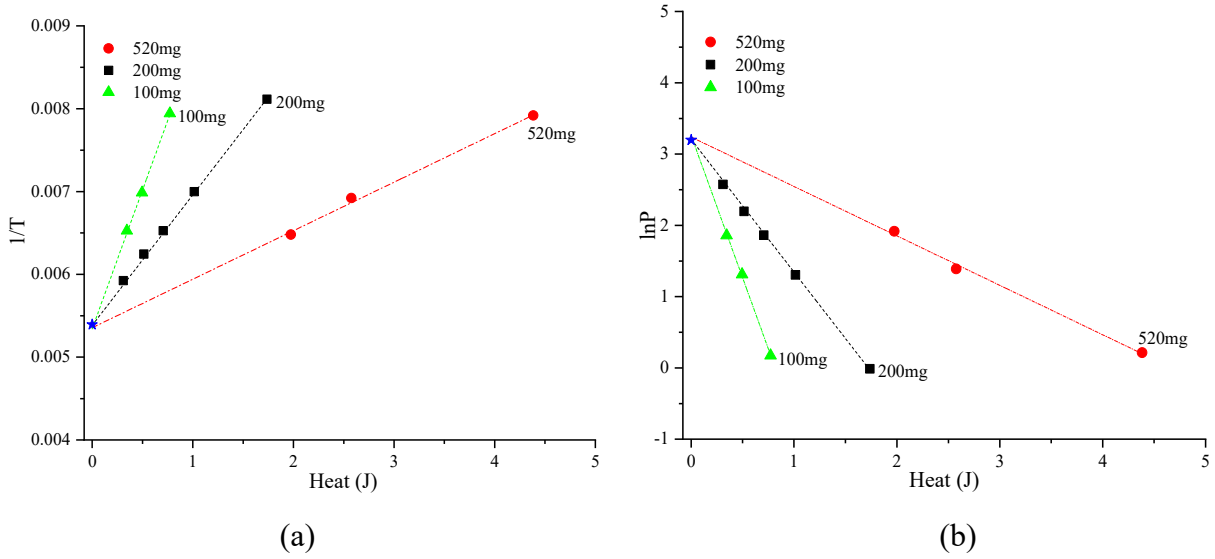

Figure 5. Three-line approach for determining (a) pore critical temperature and (b) pore critical pressure for methane in MCM-41.

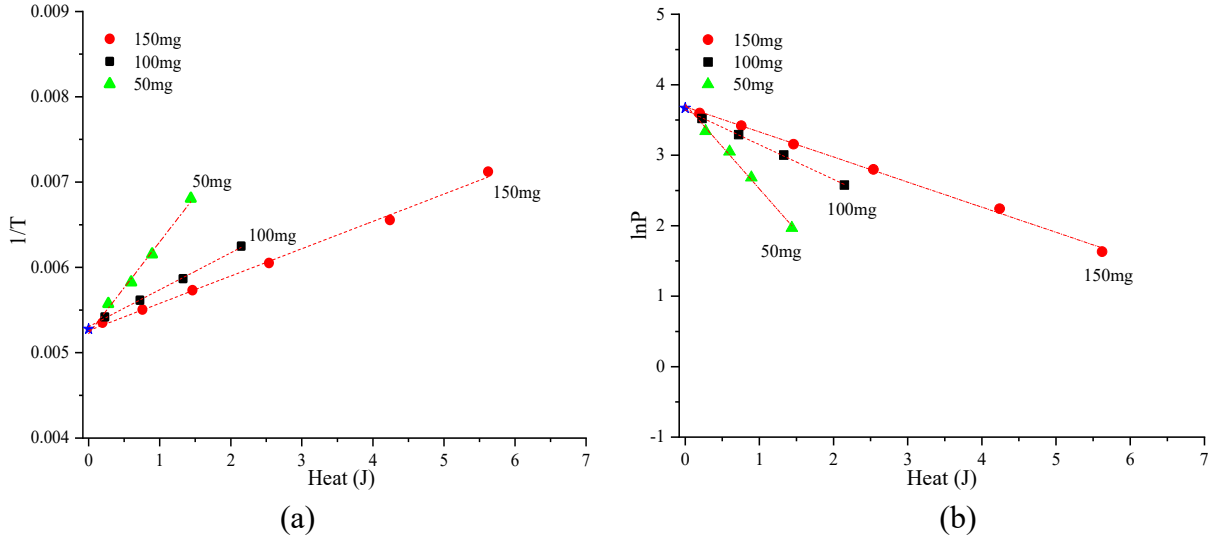

Figure 6. Three-line approach for determining (a) pore critical temperature and (b) pore critical pressure for methane in SBA-15.

Table 2. Bulk critical point, PCP, and modeling parameters for methane in MCM-41 and SBA-15

Bulk critical point from NIST		Nanopore	Pore critical point[§]		C_O	ε_p/k (K)	b
Temperature (K)	Pressure (bar)		Temperature (K)	Pressure (bar)			
190.564	45.992	MCM-41 (3.5 nm)	$185.4^{+0.8}_{-1.0}$	$24.5^{+0.7}_{-0.9}$	4.671	274.163	0
		SBA-15 (7.0 nm)	$189.5^{+1.3}_{-0.5}$	$39.2^{+1.2}_{-0.6}$	4.815	217.710	0.215

[§]The superscript and subscript denote upper and lower error, respectively.

We can conclude from Table 2 and Figure 4 that the shift of PCP from the bulk critical point for methane in MCM-41 is larger than that in SBA-15 due to the smaller pore size of MCM-41 thus stronger confinement effect. In addition, the shift of pore critical pressure is larger than that of pore critical temperature for methane in both nanopores, as found before.[17] As seen in Table 2, the pore critical pressures are much lower than the bulk critical pressure.

The uncertainties of the critical properties are derived from the linear regressions in the three-line approach, which results in asymmetric errors as presented in Table 2. With these errors, the pore critical temperature (T_{Cp}) is undoubtedly below the bulk critical temperature (T_C) for methane in MCM-41, but not for T_{Cp} in SBA-15, the upper bound of which exceeds T_C (190.8 K > 190.564 K). As T_{Cp} is conventionally believed to be lower than T_C for any porous media, the upper bound may be a reminiscence of non-idealities during experiments. Nevertheless, the finding is open for further investigation. The determination of the uncertainties is given in the Supporting Information.

5.4. Prediction Using EOS Based on the Generalized vdW Partition Function

The needed bulk parameters for methane are as follows: $m = 1$, $\sigma = 3.297$ Å, $\varepsilon/k = 130.521$ K, and $\lambda = 1.5942$, which are those of SAFT2 EOS.[31] The parameters for the confined fluid, C_o and ε_p, are then derived from the pore critical point data using the equations presented in Figure S1 in the Supporting Information, and are listed in Table 2.

The capillary-condensation for methane in MCM-41 is predicted using $b = 0$, thus the original procedure presented by Adidharma and Tan,[10] and presented on a P-T diagram in Figure 7. The AAD and ARD are 0.19 bar and 8.1%, respectively. From these results, we can conclude that the EOS well predicts the capillary condensation data of methane in MCM-41.

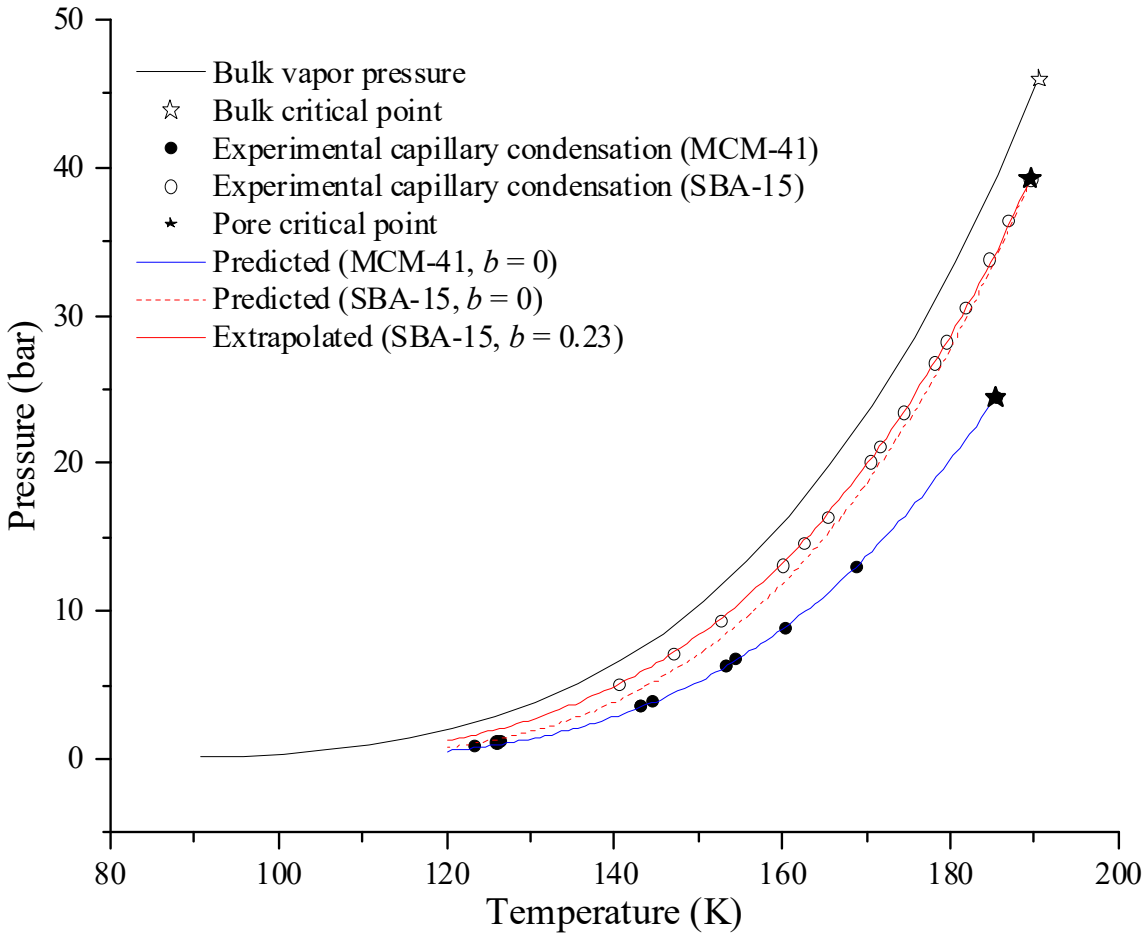

Figure 7. Model predictions of capillary condensation of methane in MCM-41 and SBA-15.

For the capillary-condensation of methane in SBA-15, the model with temperature-independent parameter C_0 in Eq (2), or Eq (1) with $b = 0$, does not well represent the experimental data, as shown in Figure 7. To obtain the correction factor b, we could use one of the experimental data points and use the result for extrapolation to the whole set of data. For example, the value of b using the capillary condensation point at $T = 174.4$ K and $P_{b\text{-}cc} = 23.50$ bar is 0.23. The calculated capillary condensation in a P-T diagram using this value of b is also shown in Figure 7. The AAD and ARD are 0.16 bar and 0.7%, respectively. We find that the modified equation works well to represent the capillary condensation data of methane in SBA-15 provided that the parameter C is made temperature dependent, which may be proposed as the generalized version of the parameter for any porous media. Whether or not the correction factor b is a constant for a certain type of adsorbent still needs further investigation in our future work.

6. Conclusions

For the first time, the capillary condensation of methane confined in mesoporous silica MCM-41 and SBA-15 is successfully measured using an experimental system utilizing a BT 2.15

DSC with isochoric procedure, the accuracy of which is confirmed by the fact that the measured bulk condensation of methane is in excellent agreement with the literature data from NIST.

The location of PCP of methane in both nanopores, which is determined using the three-line approach, is at a lower pressure and a lower temperature than the bulk critical point, with pressure shifting more than temperature. However, as the upper bound of T_{Cp} in SBA-15 exceeds T_C, the statement is open for future evaluation.

By using the EOS based on the Generalized vdW partition function, the capillary condensation conditions of methane in MCM-41 and SBA-15 are well predicted and extrapolated, respectively, and in a good agreement with experimental data. For the capillary condensation of methane in SBA-15, unlike that in MCM-41, the model parameter C is found to be a function of temperature with a correction factor that still needs further investigation on its behavior.

Conflicts of interest

There are no conflicts to declare.

Supporting Information

The Supporting Information contains experimental data of capillary condensation for determining T_{Cp} and P_{Cp}, the procedure of calculating the capillary condensation of methane in MCM-41, and the uncertainties of the experimental data.

Acknowledgments

This material is based upon work supported by the U.S. Department of Energy, Office of Science, Office of Basic Energy Sciences under Award Number DE-SC0021318.

References

1. S. Beg, M. Rahman, A. Jain, S. Saini, P. Midoux, C. Pichon, F. J. Ahmad and S. Akhter, Nanoporous metal organic frameworks as hybrid polymer–metal composites for drug delivery and biomedical applications, Drug Discovery Today, 2017, **22**, 625-637.
2. T. M. N. Albayati, S. E. Wilkinson, A. A. Garforth and A. M. Doyle, Heterogeneous alkane reactions over nanoporous catalysts, Transport in Porous Media, 2014, **104**, 315–333.
3. Z. Wang, A. Knebel, S. Grosjean, D. Wagner, S. Bräse, C. Wöll, J. Caro and L. Heinke, Tunable molecular separation by nanoporous membranes, Nature Communications, 2016, **7**, 13872.
4. H. Furukawa and O. M. Yaghi, Storage of hydrogen, methane, and carbon dioxide in highly porous covalent organic frameworks for clean energy applications, The Journal of the American Chemical Society, 2009, **131**, 8875-83.

5. L. Charlet, P. Alt-Epping, P. Wersin and B. Gilbert, Diffusive transport and reaction in clay rocks: A storage (nuclear waste, CO_2, H_2), energy (shale gas) and water quality issue, Advances in Water Resources, 2017, **106**, 39-59.
6. L. He, H. Mei, X. Hu, M. Dejam, Z. Kou, and M. Zhang, Advanced flowing material balance to determine original gas in place of shale gas considering adsorption hysteresis, SPE Reservoir Evaluation and Engineering, 2019, **22**, 1282-1292.
7. M. Polak and L. Rubinovich, Adsorption under nanoconfinement: a theoretical–computational study revealing significant enhancement beyond the Langmuirian levels, Physical Chemistry Chemical Physics, 2020, **22**, 19600-19605.
8. S. Ok, B. Hwang, T. Liu, S. Welch, J. M. Sheets, D. R. Cole, K. H. Liu, and C. Y. Mou, Fluid behavior in nanoporous silica, Frontiers in chemistry, 2020, **8**, 734.
9. F. Casanova, C. E. Chiang, C. -P. Li, I. V. Roshchin, A. M. Ruminski, M. J. Sailor and I. K. Schuller, Effect of surface interactions on the hysteresis of capillary condensation in nanopores, Europhysics Letters, 2008, **81**, 26003.
10. H. Adidharma and S. P. Tan, Prototype equation of state for phase transition of confined fluids based on the Generalized van der Waals partition function, The Journal of Chemical Physics, 2021, **154**, 111104.
11. N. S. Alharthy, T. N. Nguyen, T. W. Teklu, H. Kazemi and R. M. Graves, Multiphase compositional modeling in small-scale pores of unconventional shale reservoirs, SPE Annual Technical Conference and Exhibition, New Orleans, LA, 30 September–2 October, SPE 166306, 2013.
12. L. Jin, Y. Ma and A. Jamili, Investigating the effect of pore proximity on phase behavior and fluid properties in shale formations, SPE Annual Technical Conference and Exhibition, New Orleans, LA, 30 September–2 October, SPE 166192, 2013.
13. X. Qiu, H. Yang, M. Dejam, S. P. Tan and H. Adidharma, Experiments on the capillary condensation/evaporation hysteresis of pure fluids and binary mixtures in cylindrical nanopores, The Journal of Physical Chemistry C, 2021, **125**, 5802-5815.
14. X. Qiu, S. P. Tan, M. Dejam and H. Adidharma, Binary fluid mixtures confined in nanoporous media: Experimental evidence of no phase coexistence, Chemical Engineering Journal, 2021, **405**, 127021.
15. X. Qiu, S. P. Tan, M. Dejam and H. Adidharma, Isochoric measurement of the evaporation point of pure fluids in bulk and nanoporous media using differential scanning calorimetry, Physical Chemistry Chemical Physics, 2020, **22**, 7048-7057.
16. X. Qiu, S. P. Tan, M. Dejam and H. Adidharma, Experimental study on the criticality of a methane/ethane mixture confined in nanoporous media, Langmuir, 2019, **35**, 11635-11642.

17. S. P. Tan, X. Qiu, M. Dejam and H. Adidharma, Critical point of fluid confined in nanopores: Experimental detection and measurement, The Journal of Physical Chemistry C, 2019, **123**, 9824-9830.

18. X. Qiu, S. P. Tan, M. Dejam and H. Adidharma, Simple and accurate isochoric differential scanning calorimetry measurements: Phase transitions for pure fluids and mixtures in nanopores, Physical Chemistry Chemical Physics, 2019, **21**, 224-231.

19. S. Luo, J. L. Lutkenhaus and H. Nasrabadi, Use of differential scanning calorimetry to study phase behavior of hydrocarbon mixtures in nano-scale porous media, Journal of Petroleum Science and Engineering, 2018, **163**, 731-738.

20. S. Luo, J. L. Lutkenhaus and H. Nasrabadi, Experimental study of pore size distribution effect on phase transitions of hydrocarbons in nanoporous media, Fluid Phase Equilibria, 2019, **487**, 8-15.

21. B. Bao, S. H. Zandavi, H. Li, J. Zhong, A. Jatukaran, F. Mostowfi and D. Sinton, Bubble nucleation and growth in nanochannels, Physical Chemistry Chemical Physics, 2017, **19**, 8223-8229.

22. K. Morishige, H. Fujii, M. Uga and D. Kinukawa, Capillary critical point of argon, nitrogen, oxygen, ethylene, and carbon dioxide in MCM-41, Langmuir, 1997, **13**, 3494–3498.

23. G. Günther, J. Prass, O. Paris and M. Schoen, Novel insights into nanopore deformation caused by capillary condensation, Physical Review Letters, 2008, **101**, 086104.

24. W. -S. Chiang, E. Fratini, P. Baglioni, J. -H. Chen and Y. Liu, Pore size effect on methane adsorption in mesoporous silica materials studied by small-angle neutron scattering, Langmuir, 2016, **32**, 8849-8857.

25. K. Morishige and Y. Nakamura, Nature of adsorption and desorption branches in cylindrical pores, Langmuir, 2004, **20**, 4503-4506.

26. S. P. Tan and M. Piri, Equation-of-state modeling of confined-fluid phase equilibria in nanopores, Fluid Phase Equilibria, 2015, **393**, 48–63.

27. H. Sun and H. Li, Phase-behavior modeling of hydrocarbon fluids in nanopores using PR-EOS Coupled with a Modified Young–Laplace Equation, ACS Omega, 2020, **5**, 15177–15191.

28. B. Nojabaei, R. T. Johns and L. Chu, Effect of capillary pressure on phase behavior in tight rocks and shales, SPE Reservoir Evaluation & Engineering, 2013, **16**, 281–289.

29. E. W. Lemmon, M. O. McLinden, D. G. Friend, Thermophysical Properties of Fluid Systems. In NIST Chemistry WebBook, NIST Standard Reference Database Number 69; P. J. Linstrom, W. G. Mallard, Eds., National Institute of Standards and Technology (NIST): Gaithersburg, MD, 2017; DOI: 10.18434/T4D303 (accessed Nov 2021).

30. X. Qiu, S. P. Tan, M. Dejam and H. Adidharma, Novel isochoric measurement of the onset of vapor–liquid phase transition using differential scanning calorimetry, Physical Chemistry Chemical Physics, 2018, **20**, 26241-26248.

31. S. P. Tan, X. Ji, H. Adidharma and M. Radosz, Statistical associating fluid theory coupled with restrictive primitive model extended to bivalent ions. SAFT2: 1. Single salt + water solutions, The Journal of Physical Chemistry B, 2006, **110**, 16694–16699.

32. M. Thommes, K. Kaneko, A. V. Neimark, J. P. Olivier, F. Rodriguez-Reinoso, J. Rouquerol and K. S. W. Sing, Physisorption of gases, with special reference to the evaluation of surface area and pore size distribution (IUPAC Technical Report), Pure and Applied Chemistry, 2015, **87**, 1051-1069.

TOC:

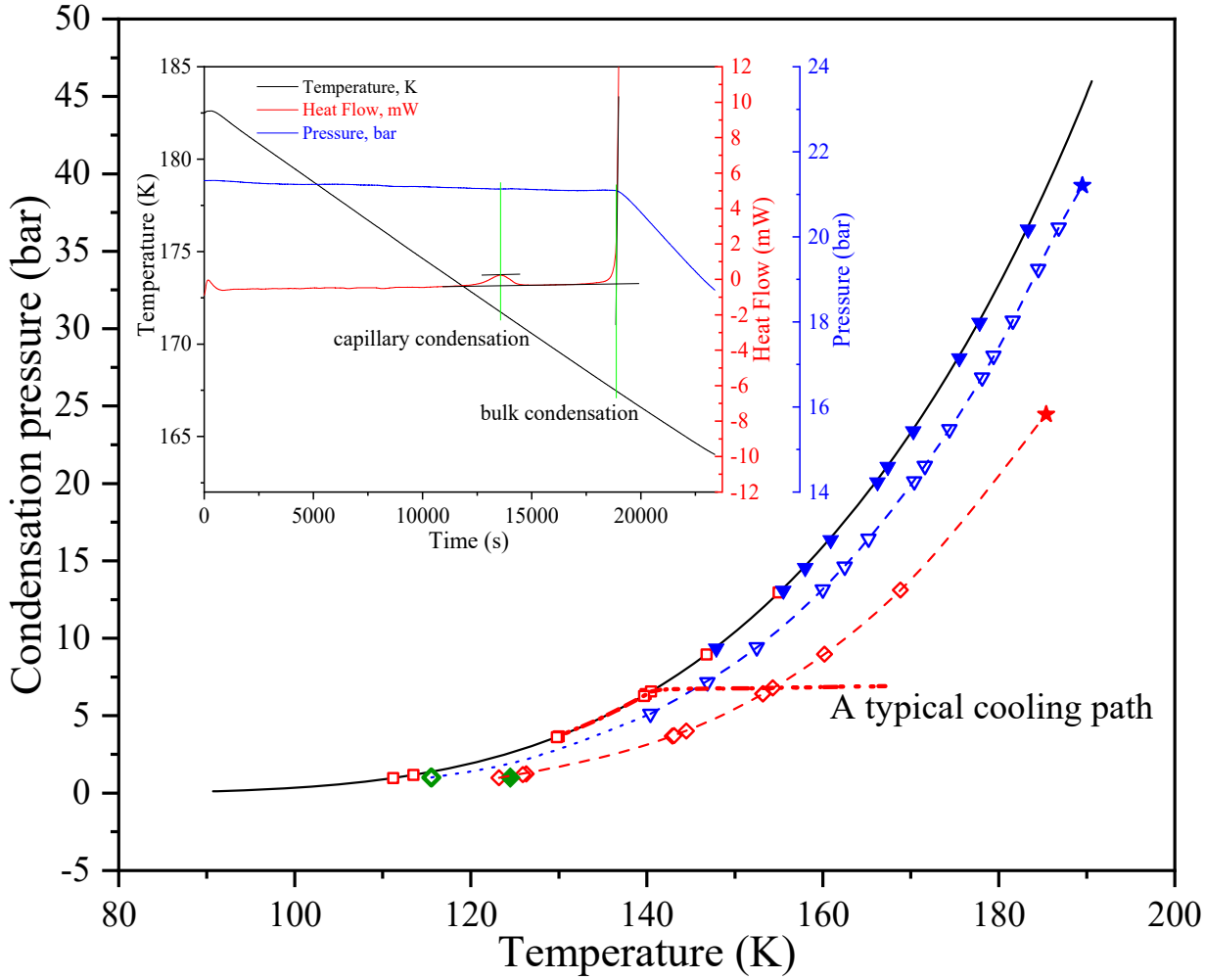
Condensation pressure (bar)
Temperature (K)
A typical cooling path
Temperature, K
Heat Flow, mW
Pressure, bar
Temperature (K)
Heat Flow (mW)
Pressure (bar)
Time (s)
capillary condensation
bulk condensation